scientific reports

OPEN

Mechanical and microstructural performance evaluation for cement-based mortar: calcined mud powder

Zafer Kurt

Although there are ongoing studies on innovative green materials, building materials are mostly composed of cementitious compounds as binders. Cement is known to significantly increase CO_2 emissions both during its production and utilization. Furthermore, while the utilization of industrial by-products in waste storage and disposal processes offers positive contributions to the circular economy, this approach does not constitute a holistic and adequate solution in terms of the environment and human health. This study presents the results of the effect of mud powder obtained from Rize province on the mechanical and microstructural properties of cement mortars to the academic environment. The mud was dried and ground, then calcined at 600, 700 and 800 °C. The calcined mud powder obtained at the optimum calcination temperature was substituted into cementitious mortars at 0%, 10%, 20%, 30% and 40% by weight. The parameters used in the study were material/ball weight = 1/12 and binder/cement weight = 0.45. Compressive and flexural tests were performed for mechanical strength and XRD, SEM–EDS, FTIR, Specific gravity, and UPV tests were performed to explain the microstructures. The numerical and test data imply that the maximum 28-day compressive strength of 46. 65 MPa was obtained as a result of 10% substitution of calcined mud powder, which is a natural resource. These results indicated that calcined powder mud (CPS) has strong potential as a sustainable material for construction and structural applications.

Keywords Mud powder, Supplementary cementitious material, Calcination, Compressive strength, XRD, Numerical analysis

The Global Cement and Concrete Association explains today's massive use of concrete with the following data approximately 14 billion m^3 of concrete is used globally every year[1]. Considering the current world population in 2024, the annual per capita concrete use is 1.72 m^3[2]. However, concrete requires a binder material to be manufactured, the most common of which has been cement since the 1800s. Cement production is estimated to contribute about 8% to global carbon footprint emissions[3,4]. The use of concrete in such high quantities around the world, and therefore the increasing use of cement as a binder, increases the carbon footprint impact. Researchers are increasingly focusing on the use of industrial by-products and alternative materials as pozzolanic or mineral additives in cement-based systems[5–10]. This is appropriate because the human population and urbanization are increasing day by day and therefore the demand for cement is increasing in parallel. In recent years, various strategies have been proposed to reduce the environmental impact of the construction industry, with particular emphasis on material-based approaches. Among these, the use of supplementary cementitious materials (SCMs) has emerged as a key pathway. The utilization of SCMs has been shown to reduce the consumption of conventional cement while enhancing the structural and functional performance of concrete[11–13].

More specifically, the incorporation of SCMs in cement-based mixtures contributes to the formation of additional hydration products during the chemical reaction process[14,15]. Their higher specific surface area improves the contact efficiency during hydration[16,17], while their filling effect enhances the density and compactness of the cementitious matrix[18,19]. Also, calcined mud powder (CPS) may exhibit similar behavior, as its pozzolanic characteristics and fine particle structure can contribute to hydration reactions and matrix densification mechanisms. Commonly used SCMs such as granulated blast furnace slag (GGBS)[20,21], fly ash (FA)[22,23], silica fume (SF)[24,25], and metakaolin (MT)[26,27] are widely adopted as partial replacements for ordinary Portland cement (OPC). However, due to increasing demand, the availability of these materials has become

Department of Civil Engineering, Recep Tayyip Erdoğan University, Fener, Rize 53100, Türkiye. email: zafer.kurt@erdogan.edu.tr

more limited, and their cost has risen in recent years[28]. For instance, limited availability of certain supplementary cementitious materials (SCMs), particularly in small quantities for research purposes, has been reported, as these materials are often produced and distributed at industrial scales. Consequently, there is an increasing need for environmentally friendly, cost-effective, and readily accessible alternative materials to partially replace ordinary Portland cement (OPC). In this context, materials that can be sourced locally and require minimal processing are considered particularly advantageous. Since such materials are often locally available, require limited logistical support, and can be supplied at relatively low cost, they offer significant potential for both the construction sector and environmental sustainability. Examples of SCMs that can be used as such natural alternatives include rice husk[29,30], palm oil[31,32], limestone calcined clays[33,34], seashell powder[35,36], and more[37–40]. However, large-scale production of such materials typically requires extensive processing, which leads to increased costs. Therefore, researchers are increasingly focusing on natural resources that require less processing and offer more economical alternatives. In recent years, studies have been carried out on the use of mud-like materials as reinforcing cementitious materials. Tang et al.[41], have studied the usability of red mud in the production of low carbon emission cements. In the study, 3 different substitution rates (15%, 30% and 45%) and calcination temperature (400 C, 600 C and 800 C) were used as parameters. They also compared the performance of red mud with blast furnace slag and fly ash, which are the most commonly used waste materials. Their findings indicate that the optimum cement composition is up to 30% substituted red mud calcined at 600 °C. Huang et al.[42], aimed to produce ultra-high performance concrete using red mud and limestone powder. For this purpose, they substituted red mud up to 30 wt% and limestone powder up to 10 wt% and determined the effect on compressive strength performance at 3, 7, 14, 28, and 56 days. The mechanical strength values they obtained show that strength above the reference value can be obtained with 10% red mud and 10% limestone substitution. Kaze et al.[43] calcined laterite soil, which is widely used in the tropics, and substituted it into Portland cementitious materials. The calcination temperature was 600 C and the substitution rates were 10, 30 and 50 wt%. As a result of the study, characterization of laterite soil substituted materials was established. In terms of mechanical strength, the data obtained show that the compressive strength decreases dramatically up to 50% substitution rate.

A considerable body of research on supplementary cementitious materials (SCMs) has focused on improving compressive and mechanical properties through the incorporation of industrial by-products into cementitious systems. However, the potential of calcined mud powder as alternative components in cement-based composites has not been sufficiently explored in the existing literature. This creates a clear gap, particularly in understanding whether such materials can provide comparable performance while offering a more accessible and sustainable option. For this reason, in this study, the mechanical properties and material characterization of the experimental groups formed by substituting calcined mud powder cementitious composite between 10–40% by weight to the control group were revealed. Additionally, researchers working on supplementary cementitous materials mostly examine the material at the micro level. The differences that the strengths they obtain cause in structural applications generally raise questions. In this study, the mechanical parameters obtained from UPV tests were used in finite element analysis, and the outputs that the parameters revealed in structural applications were examined.

Materials and methods

Materials

Cement

The binder material used in the study is CEM I 42.5 R-type cement. D_{90} granulometry parameter is 46.3 µm. The specific surface area is 1622 m^2/kg and specific gravity is 3.12 gr/cm^3. The material was supplied from Unye Cement Company See Fig. 1.

Calcined mud powder (CPS)

The calcined mud powder material was obtained from Çağırankaya locality of İkizdere district of Rize province. According to the results of the Mastersizer analysis, D_{50} granulometry parameter is 63.2 µm, the specific surface area is 687.4 m^2/kg and the specific gravity is 1.85 gr/cm^3. Table 1 demonstrates the results of XRF analysis. Also, Fig. 2 presents the particle size distributions of the cement and calcined mud powder materials used in the study. The cement sample exhibited D50 and D90 values of 13.5 µm and 46.3 µm, respectively, indicating a relatively finer particle structure. In contrast, the calcined mud powder showed larger particle sizes, with D50 and D90 values of 63.2 µm and 1310 µm, respectively. According to the XRF results, the total amount of SiO_2, Al_2O_3, and Fe_2O_3 in the calcined mud powder material was determined as 82.99%. This value is higher than the minimum limit specified for Class N pozzolans in ASTM C618 [44]. The obtained result indicates that the calcined mud powder possesses a suitable chemical composition for pozzolanic activity and may therefore be considered as a potential supplementary cementitious material in cement-based systems.

Three different temperatures, 600, 700, and 800 °C, were used for calcination. The powder sample was subjected to calcination in the furnace for 1 h to reach high temperature and 1 h under the temperature it reached. XRD patterns of the powder samples were then obtained (see Fig. 2).

Tap water

The mixing water used during the experimental program was supplied from the Building Materials Laboratory of the RTEU Technical Sciences Vocational School and complied with the requirements specified in ASTM C1602/C1602M – 22 (2022) [45], ensuring that the chemical and mechanical properties of the specimens were not adversely affected.

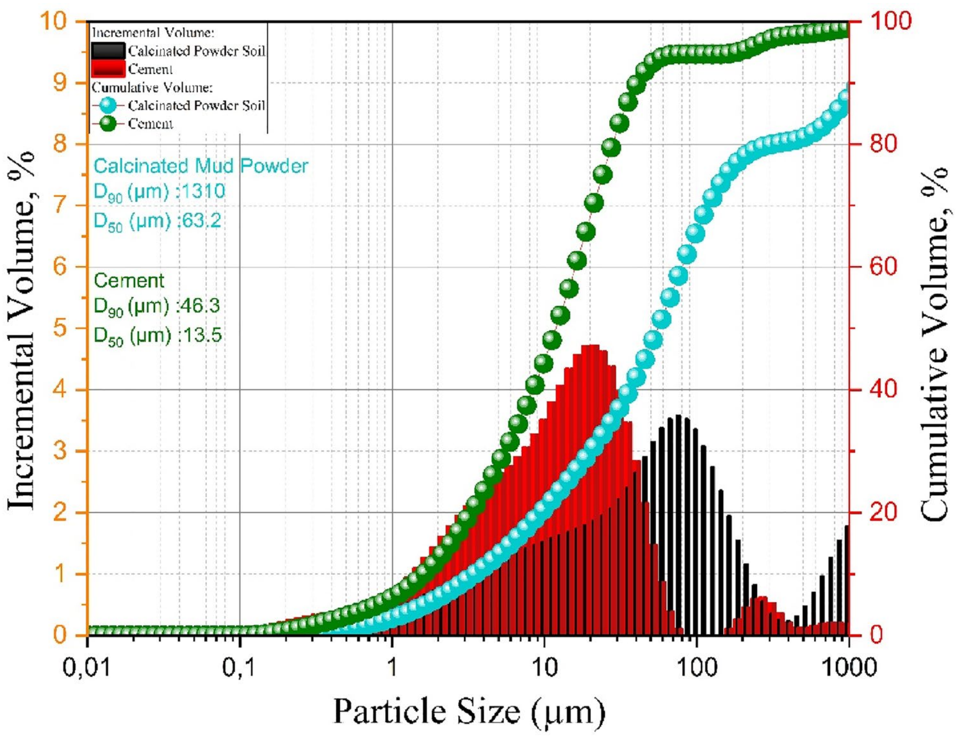

Fig. 1. Volume and particle size graph for cement and calcined mud powder.

Chemical content	Calcined Mud Powder (%)	Cement (%)
SiO_2	63.113	17.982
Al_2O_3	16.007	4.738
Fe_2O_3	3.872	3.409
K_2O	2.429	1.224
Na_2O	1.461	0.383
CaO	1.292	64.201
MgO	0.823	1.286
TiO_2	0.542	0.127
Mn_3O_4	0.084	0.059
BaO	0.057	0.067
P_2O_5	0.040	0.082
LOI	10.190	3.654

Table 1. Chemical oxide composition results.

General procedures

The experimental flowchart, including material preparation, calcination, mortar preparation, curing, and testing, is depicted in Fig. 3. The powdered material used in this study was obtained as fill soil from the Çağırankaya region of Rize province, Türkiye, and transported in sealed sacks to the Building Materials laboratory at the Recep Tayyip Erdoğan University Vocational School of Technical Sciences. Initially quite moist, the raw material (powdered soil) in the open sack was left to room temperature (22 °C ± 5 °C) for 7–10 days to remove its natural moisture content. After losing its moisture due to room temperature, the raw material was sieved through standard sieves to obtain a fine powder with particle sizes between 63 µm and 200 µm, allowing it to exhibit pozzolanic properties. The prepared powder was subjected to a calcination process at temperatures of 600 °C, 700 °C, and 800 °C. To ensure controlled heating, the furnace was allowed to reach the target temperature gradually, and the heating time was proportional to the set temperature (e.g., approximately 60 min for 600 °C; 70 min for 700 °C, and 80 min for 800 °C). After reaching the desired temperature, approximately 1 kg of powder was held at this temperature for 60 min. At the end of this period, the furnace door was opened and the material was allowed to cool rapidly at room temperature. The chemical composition and particle size distribution of the calcined mud powders were determined using XRF and laser diffraction (Mastersizer) analyses, respectively. These analyses were carried out at the Niğde Ömer Halisdemir University Central Research Laboratory. Mortar

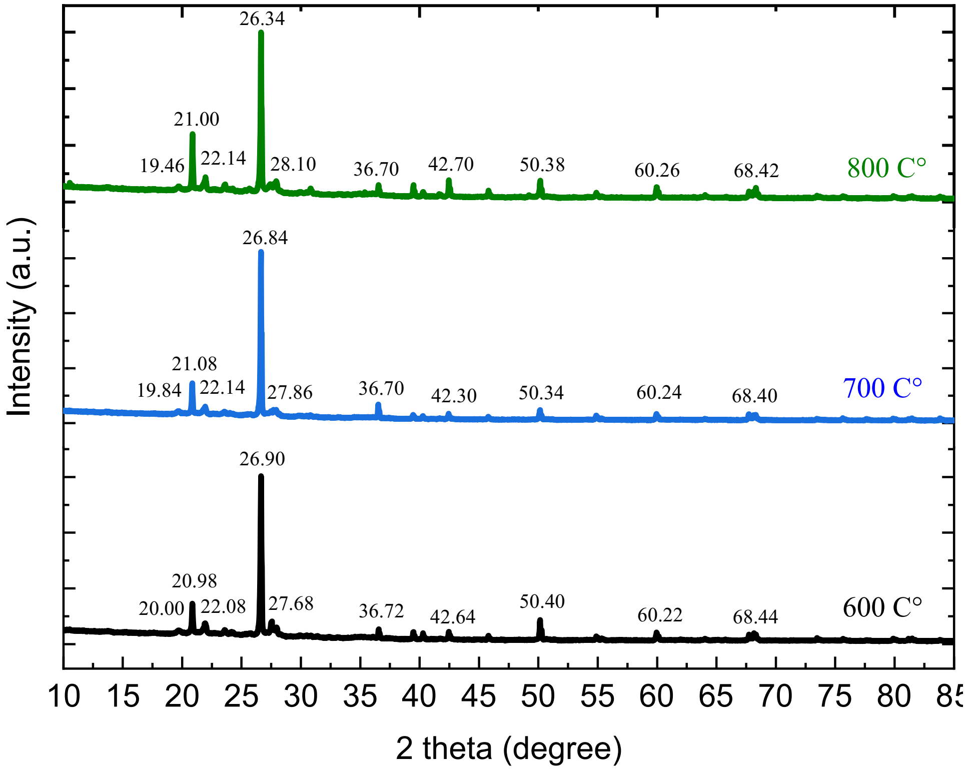

Fig. 2. XRD pattern of calcined mud powder for different temperatures.

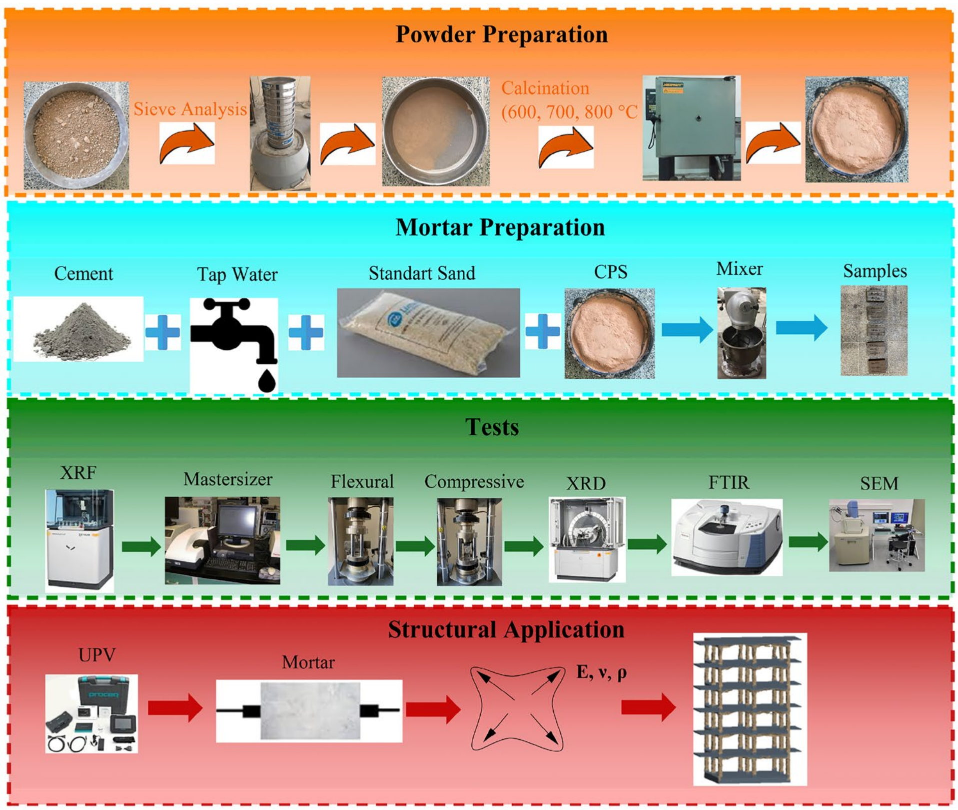

Fig. 3. Flow chart of the study conducted.

Sample Name	Tap Water (gr)	Cement (gr)	CEN Standard sand (gr)	Calcined Mud Powder (gr)	Water/ Cement
Control	202.5	450	1350	0	0.45
%10CPS	202.5	405	1350	45	0.45
%20CPS	202.5	360	1350	90	0.45
%30CPS	202.5	315	1350	135	0.45
%40CPS	202.5	270	1350	180	0.45

Table 2. Amount of materials used SCM's samples. CPS: Calcined mud powder.

CPS	Mechanical		Micro-structural					
	Flexural (7, 28 days)	Compressive (7, 28 days)	XRF	XRD (28 days)	FTIR (28 days)	SEM (28 days)	Specific Gravity (7, 28 days)	UPV (7, 28 days)
Powder	-	-	X	X	-	-	-	-
Control	X	X	-	X	X	X	X	X
%10CPS	X	X	-	X	X	X	X	X
%20CPS	X	X	-	X	X	X	X	X
%30CPS	X	X	-	X	X	X	X	X
%40CPS	X	X	-	X	X	X	X	X

Table 3. Tests for powder and mortar.

mixtures were prepared according to TS EN 196–1[46] standard using a water-cement ratio of 0.45. Fresh mixtures were poured into 40 × 160 × 160 mm rectangular prismatic molds and compacted on a vibrating table for 120 s to minimize trapped air voids. The samples were kept in the molds at room temperature for 24 h to gain their early strength, then removed from the molds. The removed samples were kept in sealed plastic bags (22 °C ± 5 °C) for curing until the day of testing. Before the test, the samples were removed from the bags. Compressive and flexural strength tests were performed on day 7 and 28. In addition, characterization techniques including XRD, SEM–EDS, FTIR, specific gravity, and ultrasonic pulse velocity (UPV) tests were applied to both powder and hardened samples. The material compositions of the mixtures are summarized in Table 2, while details of the applied test methods are given in Table 3. The abbreviation CPS is used to denote calcined mud powder.

Tests

Mechanical experiments

The samples were placed in 40*40*160 mm prismatic molds. The specimens were left in the molds for one day, then removed from the molds and stored in bags until the day of testing. The specimens that gained strength were first subjected to a bending test, and then two specimens obtained were subjected to a compression test. Three specimens were tested for each test series. The mechanical tests were conducted in accordance with the general mortar production and test standards[46,47].

XRF analysis

XRF analysis is used to determine the chemical composition of samples found in various solid, liquid, and powder forms. This analysis can quantitatively determine weights down to the ppm level in oxide or elemental form. For this purpose, a Panalytical-Zetium brand device with a 1–4 kW power amplifier and a dual-detector, which is part of the inventory of the Central Research Laboratory at Niğde Ömer Halisdemir University, was used cement and calcined mud powder (800 °C) in the production of mortar.

Mastersizer analysis

The particle size of powdered materials used in mortar production is important because it affects the mechanics of the mortar produced and the characterization of the material. For this purpose, the particle size of the cement and calcined mud powder material (800 °C) used was determined using a Zetasizer ZS90 model device at the Central Research Laboratory of Niğde Ömer Halisdemir University. The main parameters used in the device are 0–90 °C temperature, 0.3–5 nm particle size, and 0.1 ppm-40% w/v.

XRD analysis

The mortars were ground into powder in a grinder for XRD analysis. The powder samples were analyzed using the Rigaku SmartLab device (Cu-K-beta type PW1830, 2θ range: 4°–90°) located in the RTEU Central Research Laboratory. The main parameters used were 40 kV operating voltage, 0.02 step size, and 40 Ma emission.

FTIR analysis

Mortar samples for FTIR analysis were ground into powder samples in a grinder. The experiment was conducted using the Nexus 670 spectrometer device located in the Chemistry Department of RTEU. Wavelengths were scanned between 600–4000 cm-[1].

SEM–EDS analysis

Samples for SEM and EDS analysis were prepared by breaking off pieces no larger than 1 cm in diameter from locations that best represent the internal structure. The analysis was performed using an EOL JSM-6510 device located at the RTEU Central Research Laboratory. The main parameters used in the analysis were a voltage of 20 kV, a current emission of 0.9 nA, and a magnification of 5–1,000,000. Before imaging, the samples were dried in an oven to remove moisture and coated with a gold film to obtain a clear image.

UPV analysis

The homogeneity of mortars produced with ultrasonic testing devices, the distribution of cracks and voids, properties that may change over time, and dynamic physical properties can be determined. At the same time, these devices can be used to determine mechanical properties by measuring P and S waves with the help of formulas[48]. Within the scope of this study, before applying mechanical tests to mortar samples, the Proceq Pundit PL 200 device was employed to determine the ultrasonic sound velocities and mechanical properties of the samples. The P and S waves to be used in determining these properties were identified. The device consists of two 54 kHz transducers, two 250 kHz S-type transducers, and a calibration rod (25 µs). The device has two 54 kHz transducers, two 250 kHz S-type transducers, one calibration rod (25 µs), 24 kHz to 500 kHz, a measurement range of 0.1–9999 µs, and a resolution of 0.1 µs. The device can perform measurements in accordance with TS EN 12,504–4[49] and ASTM C 597–02 standards[50].

Mortar samples were placed in the device between two side surfaces, and the sound velocity and waves were measured along their length. When determining the mechanical properties (elastic modulus (E) and Poisson's ratio (µ)), the following formulas in the device's user manual were taken into account (Eq. (1), (2)) [51,52].

$$\mu = \frac{{V_P}^2 - 2{V_S}^2}{2({V_P}^2 - {V_S}^2)} \tag{1}$$

In Eq. 1, µ represents the Poisson ratio, $V_P(m/s)$ represents the primary wave velocity, and $V_S(m/s)$ represents the secondary wave velocity.

$$E(kPa) = \frac{\rho {V_S}^2 (3{V_P}^2 - 4{V_S}^2)}{({V_P}^2 - {V_S}^2)} \tag{2}$$

In Eq. 2, E (kPa) represents the elastic modulus, ρ (g/cm^3) represents the unit volume weight, V_p (m/s) represents the primary wave velocity, and V_s (m/s) represents the secondary wave velocity.

Result and discussions

Flexural strength

Figure 4a, b show the flexural strength test results for the samples after 7 and 28 days, respectively. For the 7th day, the average values obtained were 8.14 MPa for the control sample; 8.33 MPa for 10% CPS; 7.08 MPa for

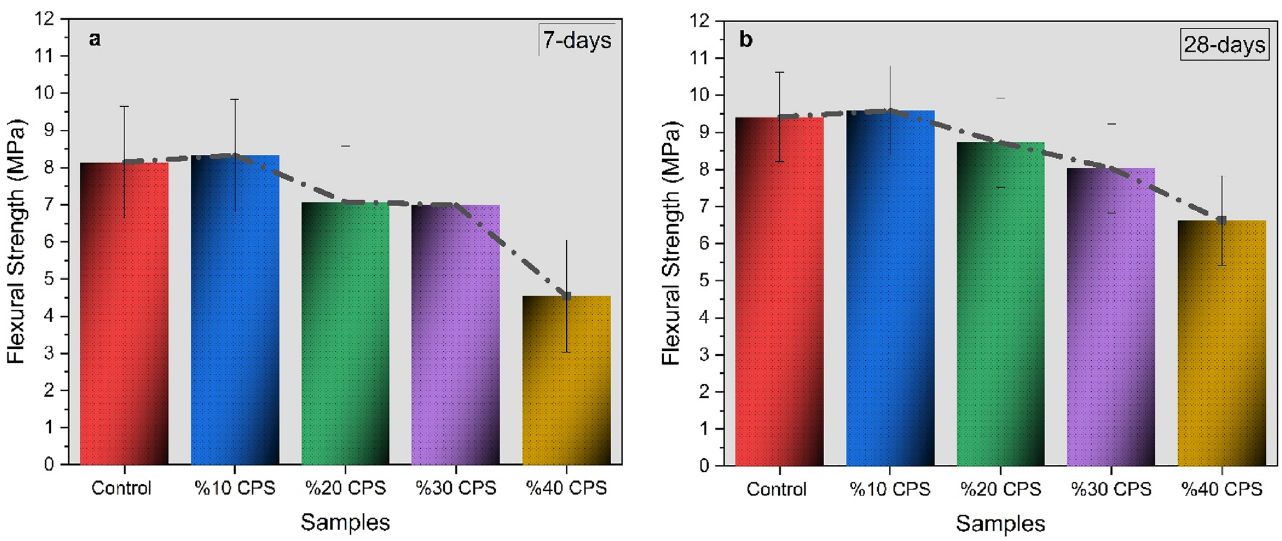

Fig. 4. Flexural strength values: (**a**)-7 days, (**b**)-28 days.

20% CPS; 6.99 MPa for 30% CPS; and 4.54 MPa for 40% CPS. Based on these values, when the control sample is taken as a reference, changes of + 2.29%, -13.06%, -14.16%, and -44.25% were observed for the other samples, respectively. In this regard, it is seen that the 10% calcined mud powder substitution improves the void structures by acting as a filler and improves the flexural strength, but substitution values between 10 and 40% reduce the flexural strength. At a 40% substitution rate, the flexural strength value is seen to drop dramatically. As is well known, for a composite or mortar material to gain strength, a gel called C-S–H must form. The increase in strength value may vary depending on the quality, density and compactness of this gel. For binding properties, CaO from limestone or chalk and minerals such as SiO_2, Al_2O_3, and Fe_2O_3 from clay-like structures react to form the gel structure called C-S–H. At a 10% substitution rate, CaO and SiO_2, Al_2O_3, and Fe_2O_3 minerals play a supplementary role in the chemical reaction. However, at a 40% substitution rate, while SiO_2, Al_2O_3, and Fe_2O_3 components are sufficiently present in the structure, the CaO content has decreased due to the reduction in the weight of the cement. This situation has relatively prevented the formation of a compact gel and caused a dramatic decrease in strength.

Saxena et al.[53] investigated the mechanical performance of cement by substituting calcined marl (CPS) at 0–40% by weight and using tap water and seawater as mixing water. Regarding flexural strength, they obtained approximately 9 MPa in the control group after 28 days. Looking at the substitution ratios, they observed a gradual decrease in flexural strength up to 40% with increasing substitution ratio in the 28-day samples. In the present study, a slight increase in flexural strength was observed with a 10% substitution ratio of CPS, followed by a gradual decrease up to 30%, and a dramatic decrease at 40%. At this point, it is seen that CPS shows similar flexural strength performance to marl for substitution ratios up to 30% (approximately 8 MPa).

Sha et al. (2024)[54] replaced cementitious materials in cement mortars with coal-based synthetic natural gas slag (CSNGS). The substitution ratio of pozzolan or supplementary cementitious materials was selected between 0–75% in this study, which is quite high. When examined in terms of comparing flexural strengths, a strength of 6.8 MPa was obtained in the control group at 7 days, while 10% slag substitution did not change this value. However, a 24% decrease was observed at a 40% substitution ratio. Furthermore, a sharp decrease was found at substitution rates of 40–75% because sufficient minerals could not be provided for adequate gel formation. At 28 days, a strength of 8.3 MPa was achieved for the control group, while a strength of 8.7 MPa was reached under the condition of 10% slag substitution. The reason why the strength values obtained in this study for the control group strengths are higher than the strengths in the specified study is attributed to the different water/binder ratio. The flexural strength for the CPS material at a 10% substitution rate was 23% higher at 7 days and 10% higher at 28 days, respectively.

Yannick et al. (2023)[55] added leaded glass powder as a SCM's to cementitious composites at substitution rates of up to 35%, replacing cement. In addition to conducting numerous environmental and chemical tests, they also examined this pozzolan material with mechanical tests. The flexural strengths for 7 and 28 days in the control group were between 6 and 7 MPa, respectively. When comparing the performance of pozzolans between studies, differences of up to approximately 45% emerge. This clearly demonstrates the pozzolanic activity and flexural strength performance of CPS's. Furthermore, the trend of increasing strength between 0–10% and decreasing strength between 10–35% is similar to the current study, indicating that the study was conducted in consistence with the literature.

Compressive strength

The compressive strengths obtained as the average of 5 different series and 6 different samples are given in Fig. 5a,b for 7 and 28 days. The reported strength values correspond sequentially to the Control, 10% CPS, 20% CPS, 30% CPS, and 40% CPS specimen groups throughout the discussion of the experimental results. For all series, compressive strengths of 42.68, 43.57, 41.54, 40.612, and 20.53 MPa were obtained at 7 days, respectively.

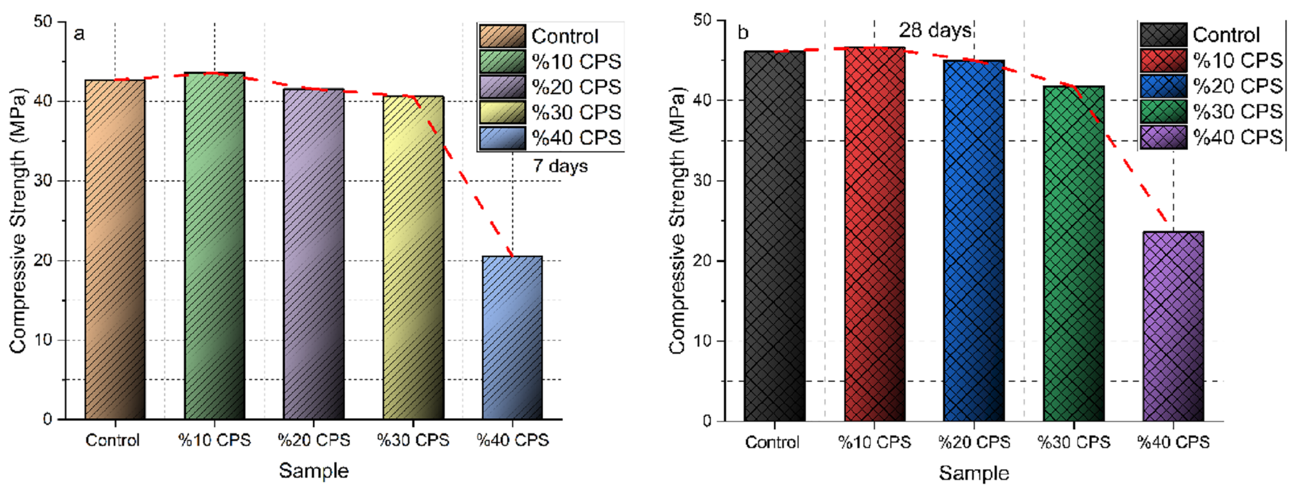

Fig. 5. Compressive strength values: (**a**)-7 days, (**b**)-28 days.

Accordingly, changes of + 2.07%, -2.67%, -4.85%, and -51.90% occurred relative to the control group. Positive development up to a 10% substitution rate in early strength was achieved with gel structures (see Fig. 5).

When the 28-day strengths were examined, values of 46.10, 46.65, 45.00, 41.74, and 23.60 MPa were obtained for all series, respectively. The tendency of pozzolan to form gel and its potential for chemical reaction can be characterized based on the strength values obtained relative to the control group. In this case, compared to the control group, the 28-day compressive strengths showed changes of + 1.20%, -3.53%, -9.45%, and -48.80%, respectively, according to the increasing substitution ratios. A sharp decline at a 40% substitution rate is noticeable as a common trend in both 7-day and 28-day strengths. It is observed that the powder material substituted with a high proportion of cement reduces the hydration product CH formed in the chemical reaction, which negatively affects the mechanical strengths[4].

In the literature, numerous studies have been conducted to improve the mechanical and/or durability properties of cement by substituting cement with different types of pozzolans at varying ratios in cement-based mixtures, thereby reducing the carbon footprint through decreased cement usage and contributing to the circular economy. Ji et al. (2025)[56] aimed to obtain low-carbon emission mixtures by substituting cement mortars with 0–40% residual tuff mud calcined powder. They observed a slight decrease at a 10% substitution rate, strength close to the control group between 10 and 30% substitution rates, and a drastic decrease at a 40% substitution rate. They also used calcination temperatures of 650–750-850 °C in their studies and stated that the 850 °C calcination temperature provided the most optimal value in terms of compressive strength. Aodkeng and Chaipanich (2025)[57] substituted three different types of calcined clay materials at 10% and 20% ratios in cement mortars. They selected a calcination temperature of 750 °C. They obtained a compressive strength above 45 MPa in the control group, which is consistent with the compressive strength obtained in the present study. The 10% calcined metakaolin substitution positively improved the compressive strength, reaching a value of approximately 55 MPa. Similarly, it was observed that replacing 10% of the control group's strength with lampang calcined clay increased the strength of the samples. In general, CPS can be used as a pozzolanic material in cement mortars in terms of mechanical strength, and the recommended substitution rate is 10%. However, at elevated substitution ratios, the added material may contribute less effectively to the hydration process and may function more similarly to a filler material within the cementitious matrix[58].

XRD analysis

XRD analysis is frequently used to determine the mineralogical composition of phases formed in cementitious mixtures. The peaks formed as a result of the analysis performed with powder samples taken from rectangular prismatic specimens may point to the formation of certain compounds[59–61]. Five different samples were scanned using an automatic database utilizing a PW1830 model with a monochromatic wavelength of λCu-K-beta at angles between 4 ~ and 90 ~ 2Θ[62]. In this context, the phases formed were determined using the QualX program[63,64]. The phase structures of the samples are shown in detail in Fig. 6 for 28-day samples.

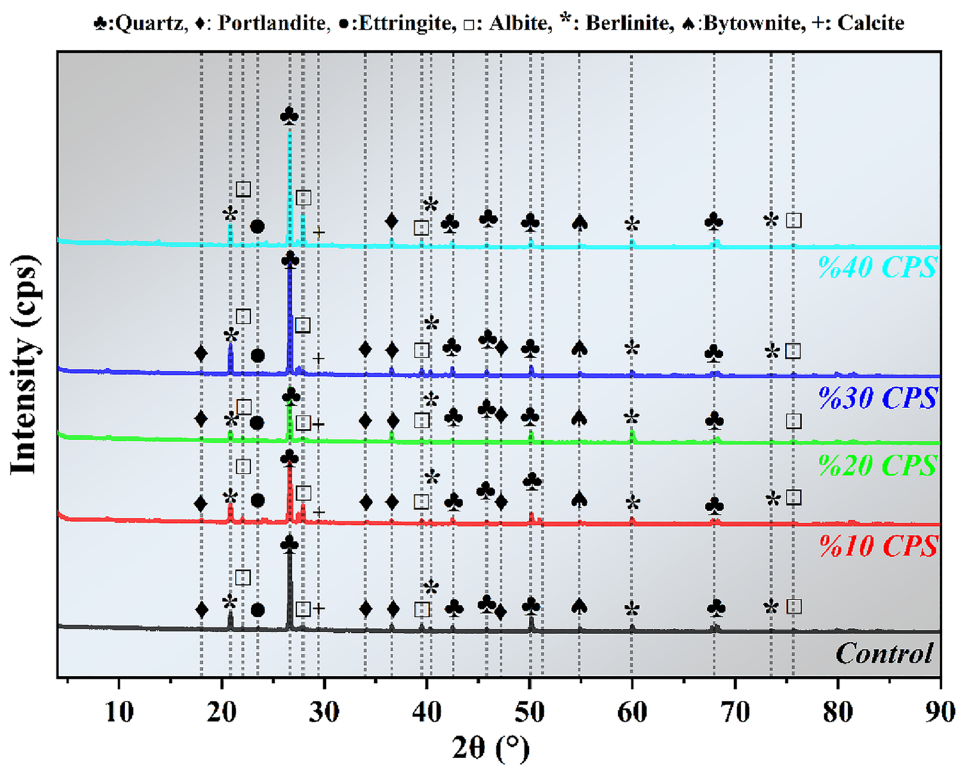

Fig. 6. XRD pattern for mortar samples.

Upon examining all samples, it is observed that the quartz mineral is dominant in the main phases. This is a normal and expected situation. Because three times the weight of standard sand was used in relation to the cement and pozzolanic material, quartz became the dominant main phase[65]. The other phases are Portlandite, Ettringite, Albite, Berlinite, Bytownite, and Calcite[66–69]. When the XRD patterns are examined, it is seen that the Portlandite peaks decrease depending on the mixtures, and the low peaks disappear. This can be attributed to the pozzolanic reaction that occurs when calcined clay is added to the mixture[59]. Following an increase in calcined clay content, the amount of Portlandite in the mixture decreases as a result of the pozzolanic reaction that occurs in the environment, and a similar situation has been demonstrated in cement pastes by Jin et al[70]. Furthermore, the main Quartz peak occurring between 20° and 30° can be attributed to the crystalline silica structure formed in all mixtures[71]. The other phases formed can be attributed to albite, berlinite glassy structure, and bytownite calcium-containing pozzolanic powder, and this is supported by XRF analysis[67,72,73]. At this point, it is observed that strength is developed in conjunction with the hydration products formed by calcium and amorphous silica content. On the other hand, it is observed that the portlandite peak disappears in samples containing 40% CPS. This can be attributed to the formation of a low amount of portlandite with the decreasing amount of cement due to the increasing amount of pozzolanic material, and the depletion of the formed portlandite structure due to its chemical reaction with the abundant pozzolanic material[74].

FTIR analysis

FTIR analysis is a method frequently preferred in microstructure analyses as it provides information about the chemical bonds within the samples. Due to the products formed as a result of cement hydration, relationships can be established with certain functional groups through wavelength-dependent bands. Figure 7 visualizes the FTIR analysis of 28-day-old samples. Also, the Fig. 7 highlights the chemical bonds that can be represented by the troughs and peaks corresponding to the refraction at different wavelengths. In addition, the transition points of the troughs in the image were zoomed in to examine the changes at the peaks of the troughs.

It is known that hydroxyl bands in clay materials are found at approximately 3600–3700 cm^{-1} [75]. O–H bands were found at a wavelength of approximately 3650 cm^{-1} in the graph. This indicates the presence of portlandite ($Ca(OH)_2$) in the structure. It is observed that this band is sharp in the control samples, but the band became straight as the clay substitution ratio rises. Furthermore, the peak of the band drops as the clay substitution ratio increases. This can be attributed to the reduction in cement in the matrix as the clay substitution ratio increases and the decrease in portlandite amount due to the increasing pozzolanic reaction. This inference is also consistent with XRD analyses. Simultaneously, this behavior may be associated with the gradual deceleration or interruption of the reaction mechanisms responsible for gel development due to the limited availability of water within the matrix. A similar tendency was also reflected in the mechanical test outcomes. In particular, the OH-related bands, which maintained a more pronounced vertical character up to 20% CPS replacement, became noticeably flatter in the mixtures containing 30% and 40% CPS. This change indicates a reduction of bound water within the structure and suggests that the loss of moisture adversely influenced the mechanical performance of the material[76]. The 1640 cm^{-1} band is the bending vibration of O–H bonds and is related to chemical hydration water[77,78], and can be attributed to the presence of water in the structure and the continuation of the reaction. The bands between 1416 cm^{-1} and 1430 cm^{-1} are related to $CaCO_3$ and the asymmetric stretching vibrations of the C–O bonds[79]. This phenomenon may indicate the presence of $CaCO_3$ in the samples, as calcite phase was detected at approximately 29° in the XRD analysis. The absorption bands around 1165, 802, 775, 749, and 692 cm^{-1} are Si–O stretching and bending bands and indicate the presence of quartz in the structure[80]. The bands at 820–1220 cm^{-1} can be attributed to [SiO_4] asymmetric stretching vibrations and are the main reaction

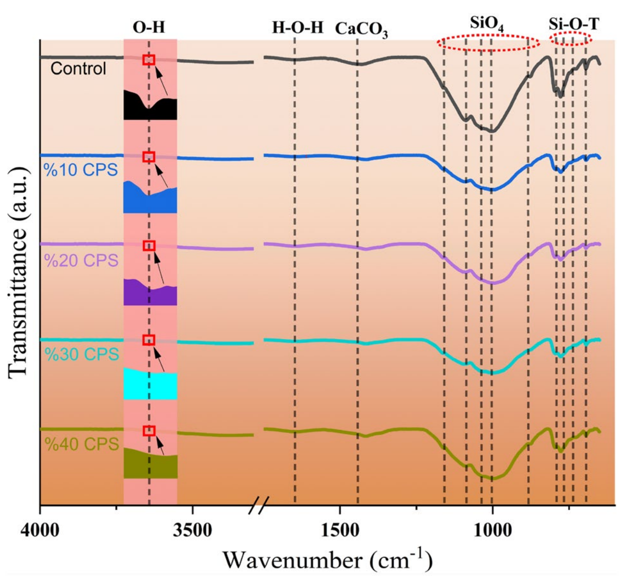

Fig.7. FTIR patterns for control and CPS samples.

bands[81]. In samples from the control group with CPS values up to 40%, it was observed that the reaction bands occurred in the range of approximately 1005–993 cm^{-1} and that the reaction bands narrowed. This phenomenon can be attributed to a decrease in the amount of amorphous silica, which inhibits pozzolanic activity[82]. The bands at 1035 and 1090 cm^{-1} can be attributed to Si–O–T (Si or Al) asymmetric stretching vibrations[82]. The bands between 700 and 820 cm^{-1} represent Si–O-Si vibrations associated with the abundant quartz in the structure[83].

Ultrasonic pulse velocity (UPV) analysis

UPV analysis is a method based on the principle of sound propagation in solid materials and voids, enabling the indirect determination of mechanical properties. The UPV values obtained for 7-day and 28-day samples are shown in Fig. 8. In the 7-day samples, changes of + 0.14%, -5.80%, -12.30%, and -29.80% were observed compared to the control group, respectively. In the 28-day samples, these changes were + 0.13%, -2.90%, -5.25%, and -26.87%. In this context, although the UPV results are indirect, they are consistent with the mechanical strengths. This is because, after the control group, it is seen that the UPV value increases with the 10% CPS substitution, depending on the filling effect of CPS. Subsequently, it is understood that as the substitution rate increases, the formation of gel structures in the matrix becomes less frequent due to the decreasing amount of cement. Along with this phenomenon, a compact structure did not form because the matrix was porous and the gel structures that participated in hydration, or even if they did, were scarce. This situation was found in the UPV values, and while the UPV values were higher in the control and 10% CPS samples, which were in a compact state, the UPV value dropped dramatically in the 40% CPS sample, which had a more porous structure. Other researchers have also noted this result in their studies. There are many studies in the literature indicating that UPV values decrease when clay materials are replaced[84,85]. For example, Padhi et al. (2023) observed that the UPV value decreased from 4830 m/s to 3200 m/s in their study where they replaced 35% of the cement with rice husk[86]. At this point, the decrease rate is 33.75%; in our study, it is 26.88% in samples containing 40% CPS. A significant part of the difference stems from the structure of the pozzolanic material used. Since each pozzolanic material inherently has different binding properties, it creates a different void structure in the mixture in which it is used. Different void structures cause different UPV values.

The relationship between the 28-day compressive strength (CS) and ultrasonic pulse velocity (UPV) values of the mixtures is presented in Fig. 9. According to the obtained results, an increase in compressive strength was generally accompanied by an increase in UPV values. The control and low-substitution mixtures exhibited higher compressive strength values in the range of approximately 42–47 MPa, while their corresponding UPV values varied between 4254 and 4496 m/s. In contrast, the mixture containing the highest replacement ratio showed a noticeable reduction in both compressive strength and ultrasonic pulse velocity values. The linear regression analysis demonstrated a strong positive relationship between CS and UPV, with a Pearson correlation coefficient close to unity (r = 0.99846) and an R^2 value of 0.99693. These findings indicate that ultrasonic pulse

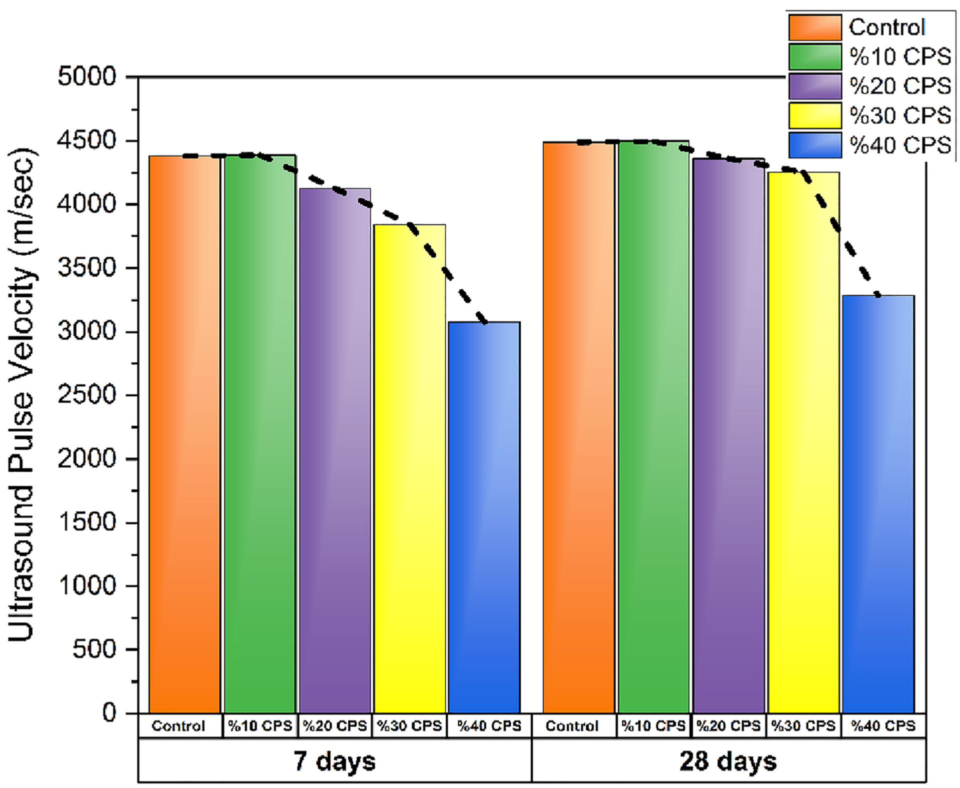

Fig. 8. Ultrasonic pulse velocity values for 7 and 28 days.

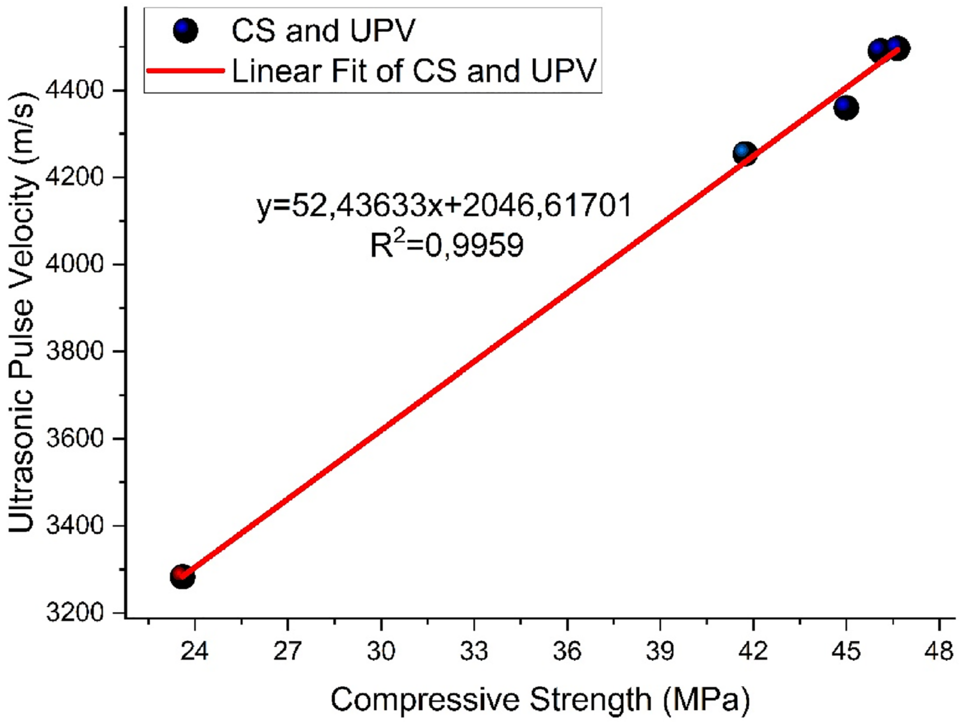

Fig. 9. Linear regression analysis for CS and UPV.

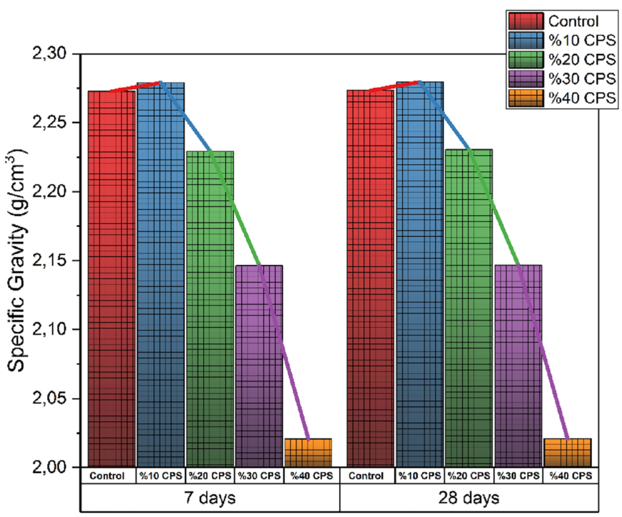

Fig. 10. Specific gravity values for 7 and 28 days.

velocity measurements were generally consistent with the compressive strength behavior of the tested mixtures and may provide indirect information regarding the internal compactness and integrity of the mortar structure.

Specific gravity

Specific gravity primarily represents a density-related physical parameter of the mixtures. However, the gels formed during hydration, including C-H, C-S–H, and C-A-S–H, may indirectly affect the compactness of the structure by contributing to a lower internal void ratio[87]. In this context, it can be predicted that mixtures with a lower void ratio will have increased mechanical strength. Figure 10 shows the specific gravities of mixtures after 7 and 28 days. It can be seen that the specific gravities of the mixtures after 7 days ranged from 2.021 to 2.272 g/cm^3. The sample containing 10% CPS has the maximum density, while the sample containing 40% CPS has the minimum density. At 28 days, there is no significant change in density, with values ranging between 2.020 and 2.273 g/cm^3. At this point, the 40% CPS substitution reduced the density by 11.08% and 11.11% for 7 and

28 days, respectively. As the CPS substitution ratio increases, the mixtures become lighter due to their inherently fine and light structure[75].

In addition to the direct influence of the constituent materials on unit density, the development of hydration products may also contribute to changes in the internal structure of the mixtures. The formation of reaction products such as C-S–H and C-A-S–H gels can partially occupy capillary spaces within the matrix and promote a more compact microstructure. This reduction in internal voids may improve particle packing and facilitate stress transfer under loading conditions. For this reason, mixtures exhibiting relatively higher specific gravity values may also present lower effective porosity and improved mechanical behavior. On the other hand, increasing CPS incorporation may alter the continuity of the cementitious matrix due to the relatively lightweight and fine nature of the material, which can result in a less compact internal structure at higher replacement levels. Therefore, the variation in specific gravity should not be evaluated solely as a physical density change, but also as an indicator of microstructural development associated with hydration reactions, pore refinement, and strength evolution within the composite system[75,88].

SEM analysis

SEM analyses were conducted on 5 different samples aged for 28 days to determine factors such as gel structures, void ratios, non-reactive or remnant materials, and macro or micro cracks that can directly affect mechanical properties. Images from the SEM analysis are provided in Fig. 11 (a-e).

In the control sample (Fig. 11a), although some C-S–H gel formation is observed in the matrix structure, the presence of particles that have not fully participated in hydration and localized micro voids is notable. However, the structure generally exhibits a more homogeneous appearance, and it is evident that the voids remain at a limited level. This indicates that the hydration products in the control mixture were able to fill the matrix to a certain extent.

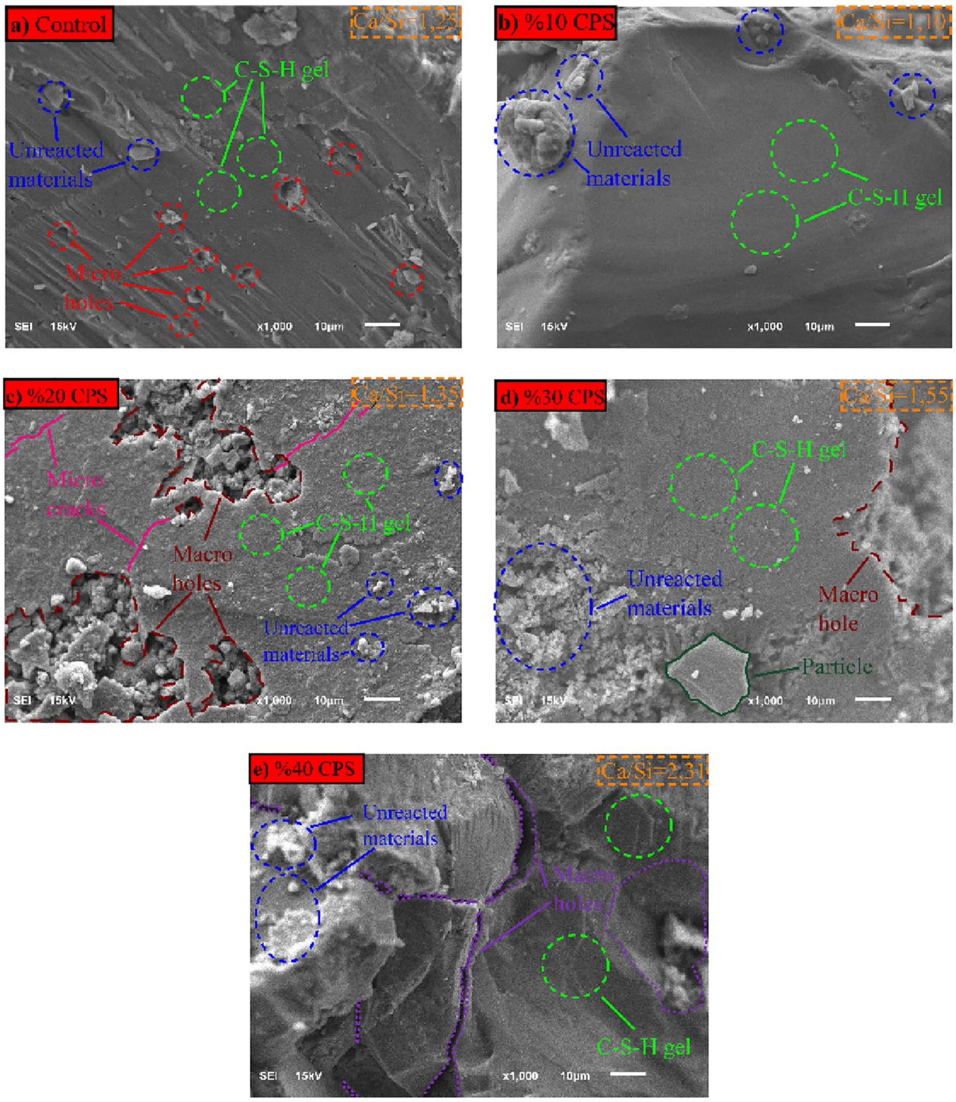

Fig. 11. SEM images for 5 different mix: (**a**) Control, (**b**) %10 CPS, (**c**) %20 CPS, (**d**) %30 CPS, and e)%40 CPS.

In the sample containing 10% CPS (Fig. 11b), the surface morphology is smoother, and the C-S–H gel phase is more widely distributed throughout the matrix. Additionally, fewer voids were observed compared to the control sample, suggesting that the hydration products form a more compact structure. However, the presence of unreacted particles in some areas is also noted. Nevertheless, the appearance of this image from the microstructure indicates that the use of low-level CPS substitution could positively affect matrix density. For mechanical strength, it was observed that gel structures were concentrated in samples replacing 10% CPS compared to the control group, voids were reduced, and it has been observed that, even though the density of non-reactive materials increases, their number decreases. In the 10% CPS samples, it is apparent from the compact structure that the void ratio decreased due to the filling effect of the pozzolanic powder material and that the pozzolanic reaction occurred more efficiently with the amorphous silica present in the structure, and this mechanism has a positive effect on mechanical strength[89].

In the sample with 20% CPS replacement (Fig. 11c), the formation of microcracks becomes more pronounced. In particular, the fact that the cracks propagate in connection with the void regions indicates that the continuity within the matrix is beginning to weaken. In addition, the increase in macro-voids and irregular porosity suggests that the distribution of hydration products within the structure has lost its homogeneity. Although the C-S–H gel phase is still present, the gel structure appears to exhibit a discontinuous character in some regions.

In the mixture containing 30% CPS (Fig. 11d), the formation of particle and extensive void regions is notable. Although the C-S–H gel structure is observed in some regions, it is evident that a heterogeneous morphology has formed throughout the matrix. The presence of unreacted large particles also indicates that the hydration mechanism was not sufficiently sustained.

In the 40% CPS sample with the highest replacement ratio (Fig. 11e), it can be seen that macro voids have become more concentrated, and unreacted particles are also noticeable. Although C-S–H gel formations have not completely disappeared, it is evident that the gel phase has been unable to form a continuous network structure within the matrix due to macro cracks. It is considered that these microstructural changes may be related to the decrease in mechanical properties observed at high CPS ratios.

Generally, in samples produced with substitution ratios above 10%, the decrease in cement content, along with reduced hydration products and particles that could not participate in the reaction, formed a matrix with a high void ratio, which negatively affected the strength values [90–92].

EDX analysis was employed to identify the Ca/Si ratios in the mixture for five different samples. An inverse relationship was observed between these identified ratios and the mechanical strength when compared to the Ca/Si ratio. Furthermore, some studies indicate that there is a significant relationship between this ratio being less than 2 and the efficiency of the pozzolanic reaction and high chemical reactivity [90,93].

Structural applications

Example 1: modal analysis

Every object inherently possesses specific vibration amplitudes. These vibration amplitudes must be known before any structure is designed. This is because if the natural frequency of the structure coincides with the frequency of external loads, a phenomenon called resonance may occur, which can theoretically increase the displacement of the system to an infinite value in damped systems [94]. To prevent this situation, modal analyses must be performed before structures are designed. Modal analysis is used in structural analyses to determine eigenfrequencies and eigenmodes. By obtaining this information, an engineer or researcher can gain insight into a structure's vibration frequencies, displacement, and damage tendencies [95].

For this purpose, modal analyses were performed using the Ansys software package, assuming that the six-storey building, whose formwork plan is given in Fig. 12, was constructed using the material whose mechanical properties are given in Table 4 [96]. The structural elements used were 60 × 60 cm columns, 30 × 60 cm beams, 15 cm high slab floors, and 80 cm high raft foundations. The floor height is 3 m.

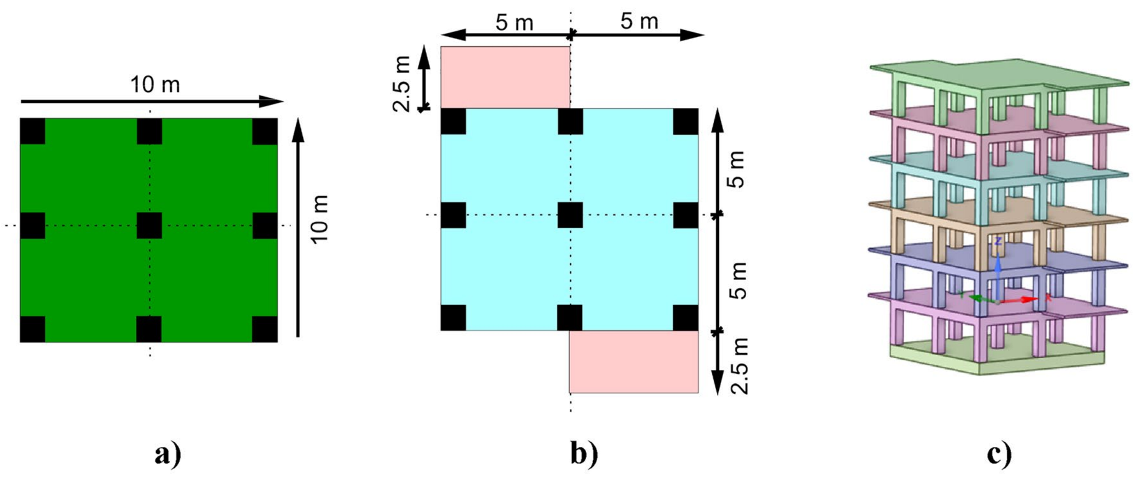

Fig. 12. Views for structure: (**a**) mat foundation, (**b**) story, (**c**) building.

Material code	Density (g/cm^3)	Elasticity modulus (MPa)	Poisson ratio
Control	2,273	39,696	0,227
%10 CPS	2,279	40,480	0,218
%20 CPS	2,230	33,228	0,279
%30 CPS	2,147	30,147	0,283
%40 CPS	2,021	16,901	0,291

Table 4. Mechanical properties for different materials.

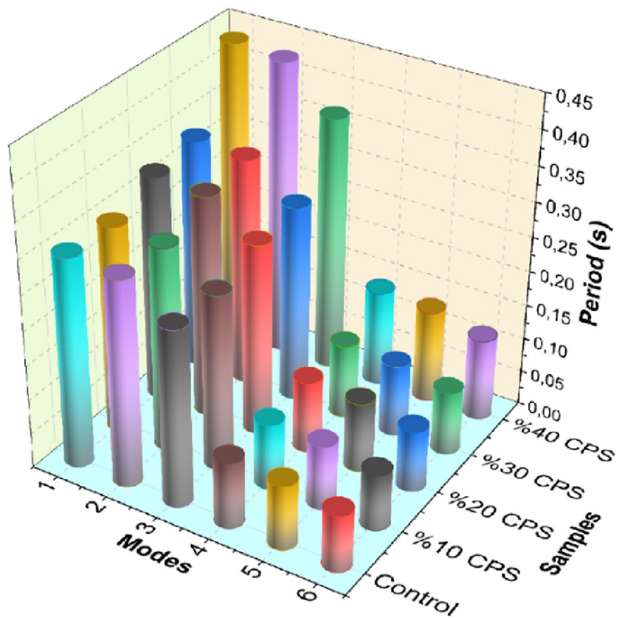

Fig. 13. Modal periods of structure for different 5 samples.

Analyses were repeated for each material code. A homogeneous linear isotropic material model was selected as the material. For the mesh method, the mesh process was completed using Patch Conforming with a mesh thickness of 300 mm. The mesh parameters are an average element quality of 0.75 and an aspect ratio of 14.5. A total of 109,170 tetrahedral elements and 204,619 nodes were used. Figure 13 shows the modal analysis results for five different material types.

When examining the values in the Fig. 13., it can be seen that for all samples, the period values decreased from the control group by up to 10% CPS from the 1st mode to the 6th mode, and increased between 10% CPS and 40% CPS. This situation corresponds to the mechanical properties. The relationship between the natural vibration period and frequency of a structure is calculated using the following equations.

$$\mathrm{T(s)} = 2\pi\sqrt{\frac{m}{k}} \tag{3}$$

f(Hz)= $\frac{1}{T}$ (4).

Here, T(s) represents the natural vibration period, f represents the frequency, m represents the mass of the structure, and k represents the stiffness of the structure. From the mechanical properties, it can be seen that the elasticity modulus increased by approximately 2% up to 10% CPS compared to the control group, then decreased by 16.3% at 20% CPS, 24% at 30% CPS, and 57.4% at 40% CPS. Since the elasticity moduli used directly affect the stiffness values, they decrease by approximately 0.8% at 10% CPS in mode 1 compared to the control group, and by 8%, 11.2%, and 44.1% in the 20% CPS and 40% CPS samples, respectively. This situation indicates that when the CPS substitution in the material increases between 10 and 40%, the rigidity of the structure decreases and the natural period, which is the time required for the structure to return to its original position, increases.

Example 2: topology optimization

Topology optimization is used to obtain the optimum material and/or section layout that maximises or minimises a predefined objective function, such as strength, natural frequency, or weight, by reducing the volume or cross-section of a part or structure[97]. In this example, the structure used in Example 1 was analysed for five different materials under seismic loading, and section optimization was performed based on the maximum compressive strength of the materials, thereby comprehensively examining the effect of the materials on the structure. For the analysis of the structure, the unscaled records of the 6.7 magnitude Northridge earthquake that occurred in California in 1994 at the Alhambra—Fremont School station (RSN 942) were selected, and the records were obtained from the PEER Ground Motion Database[98]. For the floor covering loads of the structure, 2 kN/m^2 was considered, and for the moving loads, distributed loads of 5 kN/m^2 were considered for all floors[99]. Figure 14 demonstrates the earthquake record. The ANSYS Workbench Software Package[100] was utilised for numerical analysis and for finite element method application.

Since a mesh structure is required for static analysis, a mesh was created using the Patch Independent method with a mesh size of 200 mm. A total of 269,778 elements and 501,170 nodes were used in the tetrahedral structure. The materials used are homogeneous and have linear isotropic properties. Upon examination of the analysis results, the structures were found to be safe for seismic loads in 5 different models. Following the static analysis, topology optimization was performed, with global stress selected as the objective function. Optimization was carried out on the sections, planning for the maximum global stress to correspond to the compressive strength of the material used. The images obtained from the analysis under seismic and cladding loads are shown in Fig. 15.

The analysis results show that the maximum Von Mises stress in the control group was 11.816 MPa and the minimum Von Mises stress in the 40% CPS group was 10.895 MPa. The 40% CPS substitution reduced the stress values by 7.8% compared to the control group. When examining the sample strengths obtained from the pressure resistance test, it is understood that all structural groups remained on the safe side in terms of stress analysis (see Fig. 5). The reduced sections obtained as a result of topology optimization are shown in Fig. 16.

When reviewing Fig. 16, the minimum residual volume was 93.660% in the control group, while the minimum residual volume was 93.889% in the structure using 40% CPS material. At this point, there was a volume difference of 0.229% between the control group and the 40% CPS group.

Conclusions

In this study, calcined powder soil (CPS) obtained from naturally sourced soil material was incorporated into cement mortar mixtures at substitution ratios ranging from 10 to 40%. Also, the mechanical and microstructural properties of the cement mortars were examined. The results obtained from the mechanical, microstructural, and numerical analyses were listed below.

- In mixtures with 10% CPS substitution, a maximum value of 8.33 MPa was obtained in 7 days, and 9.59 MPa in 28 days for flexural strength.
- In terms of compressive strength, mixtures with 10% CPS substitution achieved a maximum value of 43.57 MPa in 7 days and 46.65 MPa in 28 days.
- When mechanical strength is considered, although the 10–30% CPS substitution values are close to those of the control group, a dramatic decrease is observed at 40% CPS substitution.
- The presence of pozzolanic reaction occurring with the presence of CPS along with microstructural analyses has been found to be consistent with mechanical strengths.
- In all linear elastic numerical analyses conducted under seismic loads, the structures built for all substitution ratios remain on the safe side.

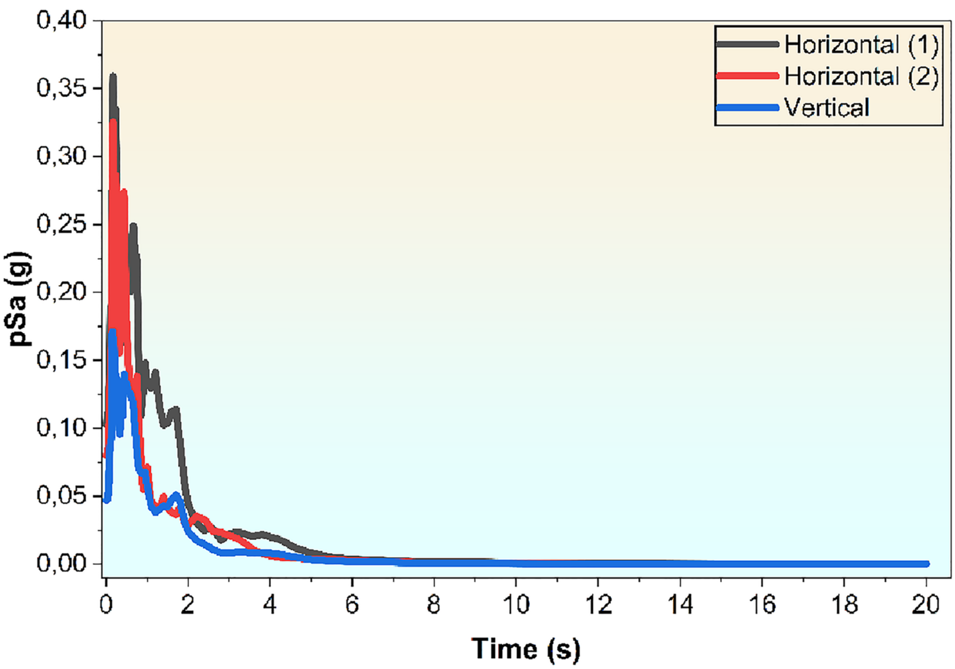

Fig. 14. Horizontal and vertical component of earthquake record for 1994 Northridge.

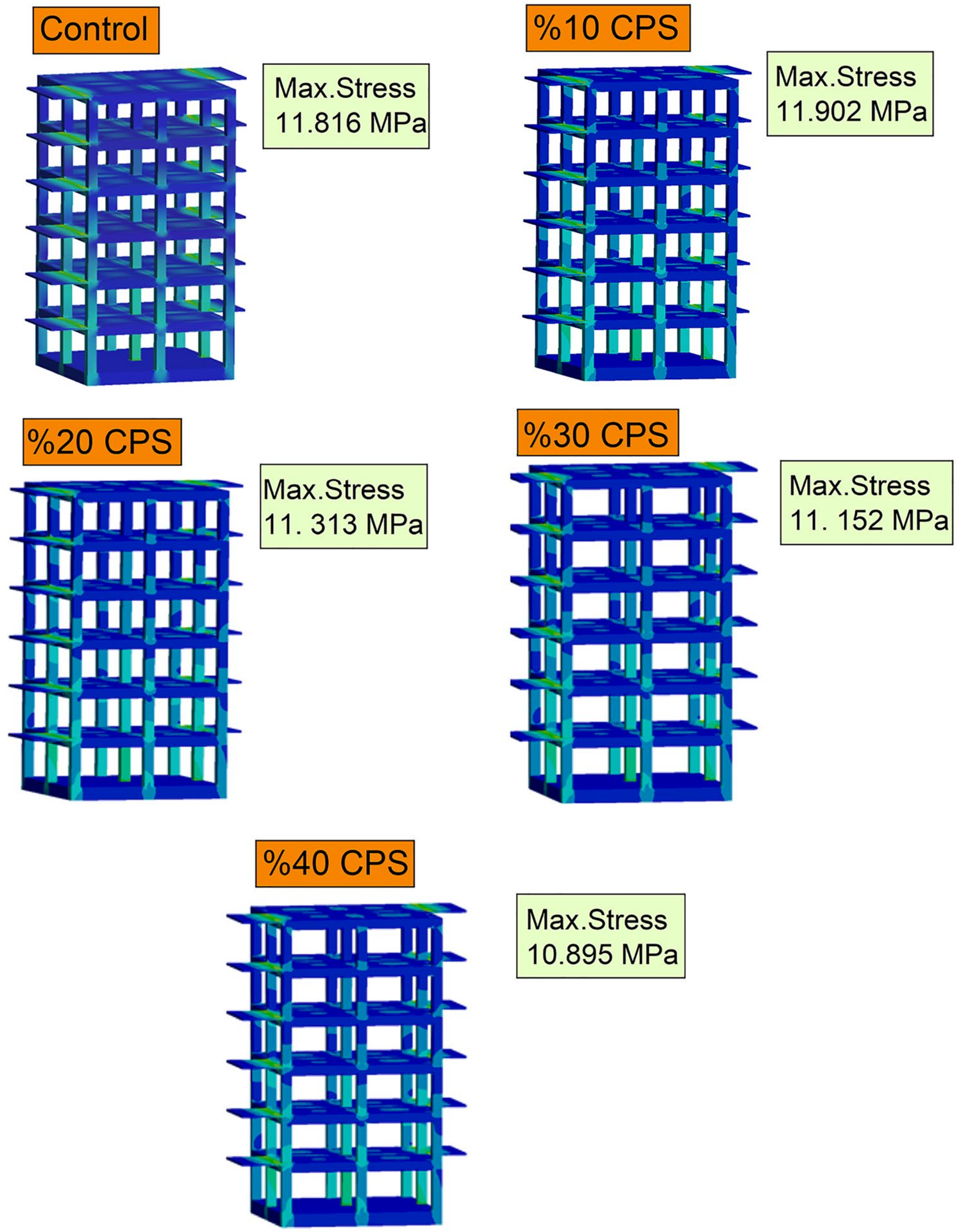

Fig. 15. Result of earthquake analysis.

- Numerical analyses and topology optimization have demonstrated that CPS can be employed as a supplementary material in cementitious composites.

Every researcher who has made it their mission to work in this field is trying to reduce the amount of cement and produce composite materials that are both load-bearing, economical, and environmentally friendly with optimized mixtures, using pozzolanic materials that can be used as a substitute, even if they cannot completely eliminate cement. With increasing studies every day, the use of cementitious materials is growing, and knowledge is accumulating through research. In this study, not only were the mechanical and microstructural properties of the pozzolanic material, deemed appropriate to be named CPS, examined, but the synergistic effect of this material in terms of structural engineering was also investigated. However, every study has certain limitations, and in this study, information regarding the performance of the specified pozzolanic material in mixtures under long-term durability effects remains unclear. The author believes that researchers conducting future studies may focus on this issue.

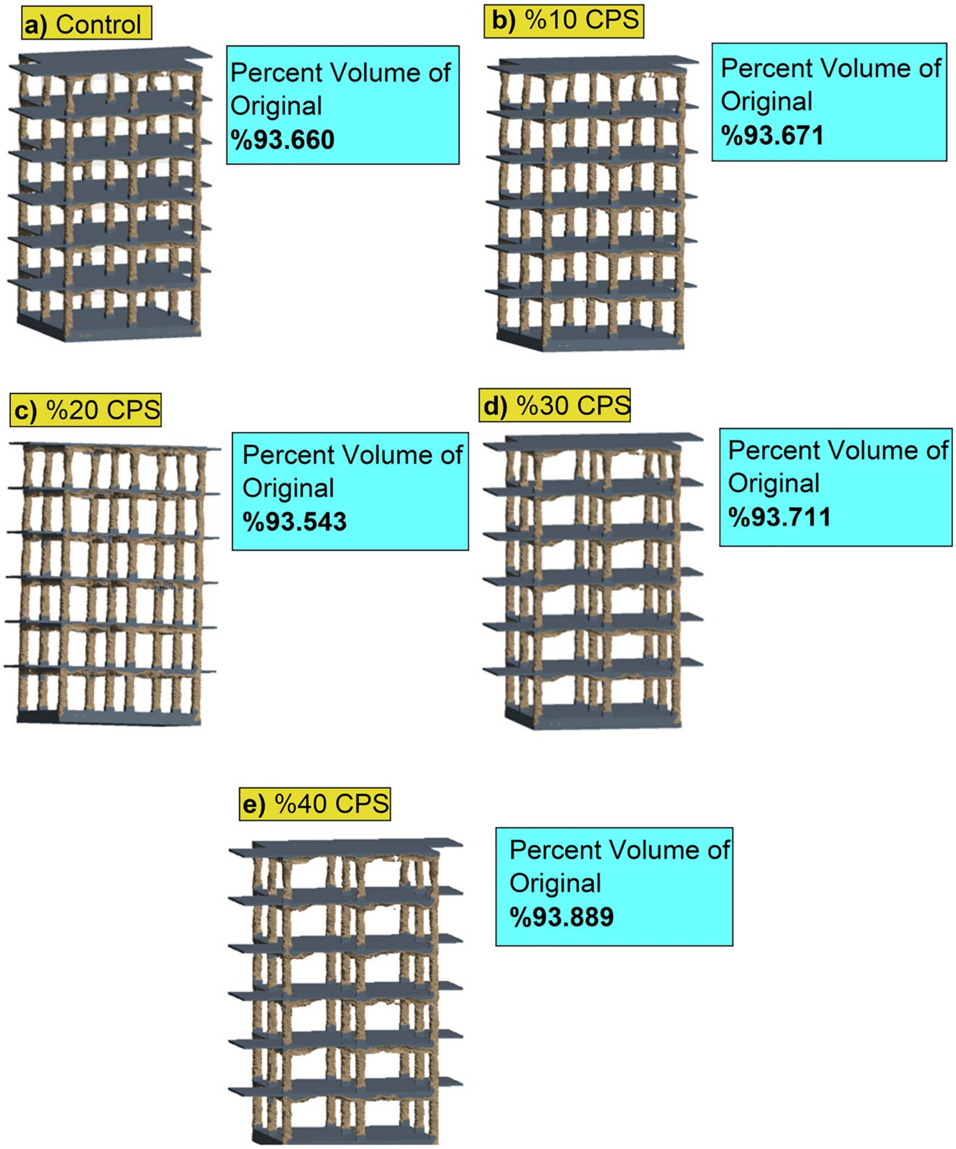

Fig. 16. Topology optimization values.

Data availability
All data generated or analyzed during this study are included in this published article.

Received: 14 February 2026; Accepted: 2 June 2026
Published online: 22 June 2026

References

1. McCaslin, E. R. & White, C. E. A parametric study of accelerated carbonation in alkali-activated slag. *Cem. Concr. Res.* **145**, 106454. https://doi.org/10.1016/j.cemconres.2021.106454 (2021).
2. Url-1: https://populationtoday.com/tr/
3. Lei, J. et al. Recycling of aluminosilicate solid wastes in a novel glass calcined clay cement (GC3). *J. Am. Ceramic Soc.* https://doi.org/10.1111/jace.20666 (2025).
4. Ahmed, H. U., Mohammed, A. A. & Mohammed, A.-S. Effectiveness of nano-SiO2 on the mechanical, durability, and microstructural behavior of geopolymer concrete at different curing ages. *Archiv.Civ.Mech.Eng* **129**, 129. https://doi.org/10.1007/s43452-023-00668-w (2023).
5. Yu, J. et al. Experimental investigation of effects of multi-fissures on brittleness of ordinary Portland cement concrete and rubberized concrete. *Eng. Fract. Mech.* **306**, 110254. https://doi.org/10.1016/j.engfracmech.2024.110254 (2024).
6. Aliha, M. R. M., Iranmanesh, M. A., Afrasiabian, A. & Mohammadi, M. H. Fracture toughness of clay stabilized with different additives: An experimental and theoretical study. *Eng. Fract. Mech.* https://doi.org/10.1016/j.engfracmech.2025.111739 (2025).
7. Wan, C. et al. The fracture performance of modified recycled concrete: Influence of recycled aggregate and recycled powder. *Eng. Fract. Mech.* https://doi.org/10.1016/j.engfracmech.2025.111709 (2025).

8. Lan, J., Dong, Y., Kai, M. F., Hou, H. & Dai, J. G. Investigation of waste alkali-activated cementing material using municipal solid waste incineration fly ash and dravite as precursors: Mechanisms, performance, and on-site application. *J. Hazard. Mater.* **465**, 133416. https://doi.org/10.1016/j.jhazmat.2023.133416 (2024).
9. Wen, B. et al. The effect of waste glass incorporation on the high-temperature resistance of cement-based concrete. *Arch. Civ. Mech. Eng.* **156**, 156. https://doi.org/10.1007/s43452-025-01206-6 (2025).
10. Kurt, Z., Yilmaz, Y., Cakmak, T. & Ustabaş, I. A novel framework for strength prediction of geopolymer mortar: Renovative precursor effect. *Journal of Building Engineering* **76**, 107041. https://doi.org/10.1016/j.jobe.2023.107041 (2023).
11. Schneider, M., Hoenig, V., Ruppert, J. & Rickert, J. The cement plant of tomorrow. *Cem. Concr. Res.* **173**, 107290. https://doi.org/10.1016/j.cemconres.2023.107290 (2023).
12. Abolhasani, A., Nazarpour, H. & Dehestani, M. Effects of silicate impurities on fracture behavior and microstructure of calcium aluminate cement concrete. *Eng. Fract. Mech.* **242**, 107446. https://doi.org/10.1016/j.engfracmech.2020.107446 (2021).
13. Albaijan, I. et al. Optimal machine learning-based method for gauging compressive strength of nanosilica-reinforced concrete. *Eng. Fract. Mech.* **291**, 109560. https://doi.org/10.1016/j.engfracmech.2023.109560 (2023).
14. Tironi, A., Trezza, M. A., Scian, A. N. & Irassar, E. F. Assessment of pozzolanic activity of different calcined clays. *Cement Concr. Compos.* **37**, 319–327. https://doi.org/10.1016/j.cemconcomp.2013.01.002 (2013).
15. Hollanders, S., Adriaens, R., Skibsted, J., Cizer, Ö. & Elsen, J. Pozzolanic reactivity of pure calcined clays. *Appl. Clay Sci.* **132**, 552–560. https://doi.org/10.1016/j.clay.2016.08.003 (2016).
16. Seraj, S., Cano, R., Ferron, R. D. & Juenger, M. C. The role of particle size on the performance of pumice as a supplementary cementitious material. *Cement Concr. Compos.* **80**, 135–142. https://doi.org/10.1016/j.cemconcomp.2017.03.009 (2017).
17. John, E., Matschei, T. & Stephan, D. Nucleation seeding with calcium silicate hydrate–A review. *Cem. Concr. Res.* **113**, 74–85. https://doi.org/10.1016/j.cemconres.2018.07.003 (2018).
18. Mehdipour, I., Kumar, A. & Khayat, K. H. Rheology, hydration, and strength evolution of interground limestone cement containing PCE dispersant and high volume supplementary cementitious materials. *Mater. Des.* **127**, 54–66. https://doi.org/10.1016/j.matdes.2017.04.061 (2017).
19. Cordeiro, G. C., Toledo Filho, R. D., Tavares, L. M. & Fairbairn, E. M. R. Pozzolanic activity and filler effect of sugar cane bagasse ash in Portland cement and lime mortars. *Cement Concrete Composites.* **30**(5), 410–418. https://doi.org/10.1016/j.cemconcomp.2008.01.001 (2008).
20. Hatefi, M. H. et al. Mechanical behavior and microstructural investigation of loess sustainable stabilization using nanosilica and GGBS. *Sci. Rep.* **16**, 4187. https://doi.org/10.1038/s41598-025-34210-0 (2026).
21. Zuaiter, M. et al. Effect of blending GGBS and silica fume on the mechanical properties of geopolymer concrete. *Sci. Rep.* **15**, 9091. https://doi.org/10.1038/s41598-025-93637-7 (2025).
22. Akhunzada, K. et al. Fracture behavior of slag/fly ash-based geopolymer mortar under different fracture modes. *Eng. Fracture Mech.* https://doi.org/10.1016/j.engfracmech.2025.111216 (2025).
23. Zhang, N. et al. Fracture properties of tailings-based geopolymer incorporated with class F fly ash under mode I loading conditions. *Eng. Fracture Mech.* **271**, 108646. https://doi.org/10.1016/j.engfracmech.2022.108646 (2022).
24. Wang, R. et al. Optimization of mix proportions and hydration study of high-strength concrete incorporating corn stalk ash and silica fume as supplementary cementitious materials. *Sci. Rep.* https://doi.org/10.1038/s41598-026-39419-1 (2026).
25. Omran, S. et al. Utilization of electronic plastic waste as fine aggregate with and without silica fume in concrete: Experimentation and life cycle assessment. *Sci. Rep.* **5723**, 5723. https://doi.org/10.1038/s41598-026-35491-9 (2026).
26. Ma, W. et al. Research on fracture damage characteristics of loess solidified with steel slag, calcium carbide slag and metakaolin. *Eng. Fract. Mech.* **289**, 109389. https://doi.org/10.1016/j.engfracmech.2023.109389 (2023).
27. Khater, H. M. & ElMoied,. Preparation and characterization of self-cured geopolymer binder using metakaolin precursor. *Sci. Rep.* **3270**, 3270. https://doi.org/10.1038/s41598-025-32571-0 (2026).
28. Dinakar, P., Sahoo, P. K. & Sriram, G. Effect of metakaolin content on the properties of high strength concrete. *Int. J. Concrete Struct. Mater.* **7**(3), 215–223. https://doi.org/10.1007/s40069-013-0045-0 (2013).
29. Raisi, E. M., Amiri, J. V. & Davoodi, M. R. Influence of rice husk ash on the fracture characteristics and brittleness of self-compacting concrete. *Eng. Fract. Mech.* **199**, 595–608. https://doi.org/10.1016/j.engfracmech.2018.06.025 (2018).
30. Ullah, M. F. et al. Modeling and optimization of sustainable ternary concrete incorporating rice husk ash and extracted micro silica. *Sci. Rep.* **5063**, 5063. https://doi.org/10.1038/s41598-026-35983-8 (2026).
31. Katte, A. R., Mwero, J., Gibigaye, M. & Koteng, D. O. Recycling palm oil wastes for the production of a pozzolanic cement replacement material for concrete. *Res. Eng.* **17**, 100903. https://doi.org/10.1016/j.rineng.2023.100903 (2023).
32. Abraham, H. B. et al. Performance evaluation of cellular lightweight concrete using palm oil industrial waste as cement and fine aggregate replacement materials. *Materials Today: Proceedings* **52**, 902–910. https://doi.org/10.1016/j.matpr.2021.10.301 (2022).
33. Mañosa, J., Calderón, A., Salgado-Pizarro, R., Maldonado-Alameda, A. & Chimenos, J. M. Research evolution of limestone calcined clay cement (LC^3), a promising low-carbon binder–A comprehensive overview. *Heliyon* **10**, e25117. https://doi.org/10.1016/j.heliyon.2024.e25117 (2024).
34. Chen, X. et al. A hybrid prediction and multi-objective optimization framework for limestone calcined clay cement concrete mixture design. *Sci. Rep.* **22120**, 22120. https://doi.org/10.1038/s41598-025-05288-3 (2025).
35. Hasan, K., Islam, T., Ferdaus, R. & Yahaya, F. M. Experimental study on environment-friendly concrete production incorporating palm oil clinker and cockle shell powder as cement partial replacement. *Mater. Today Proc.* https://doi.org/10.1016/j.matpr.2023.11.150 (2023).
36. Seesanong, S. et al. Green Ca-source of cockle shells converted to calcium acetate for environmental sustainability. *Heliyon* **10**, e32153. https://doi.org/10.1016/j.heliyon.2024.e32153 (2024).
37. Chung, S. et al. Microstructural investigation of mortars incorporating cockle shell and waste fishing net. *Case Stud. Constr. Mater.* **18**, e01719. https://doi.org/10.1016/j.cscm.2022.e01719 (2023).
38. Souidi, A. et al. The effect of mussel shell powder on the thermal and mechanical properties of plaster. *Constr. Build. Mater.* **416**, 135142. https://doi.org/10.1016/j.conbuildmat.2024.135142 (2024).
39. Huang, T. et al. Effects of steel slag content on the performance of alkali-activated coal gangue-slag mortar. *Sci. Rep.* https://doi.org/10.1038/s41598-026-38962-1 (2026).
40. Ngayakamo, B. H. & Ikotun, B. D. Utilization of quartz quarry dust as a sustainable partial sand replacement in cement mortar. *Sci. Rep.* https://doi.org/10.1038/s41598-026-37993-y (2026).
41. Tang, J., Zhou, W., Cai, X. & Zhang, D. Feasibility of upcycling red mud for low-CO_2 cement via calcination: A comparative study with FA and GGBFS based in China. *J. Clean. Prod.* **476**, 143734. https://doi.org/10.1016/j.jclepro.2024.143734 (2024).
42. Huang, Y., Chen, Q., Shang, H., Wang, J. & Song, N. Development of sustainable ultra-high-performance concrete (UHPC) by synergistic utilization of red mud and limestone powder. *J. Build. Eng.* **90**, 109372. https://doi.org/10.1016/j.jobe.2024.109372 (2024).
43. Kaze, R. C. et al. Influence of calcined laterite on the physico-mechanical, durability and microstructure characteristics of portland cement mortar. *Innov. Infrastruct. Solut.* **9**(7), 248. https://doi.org/10.1007/s41062-024-01564-9 (2024).
44. Astm, C. (2003). 618. Standard specification for coal fly ash and raw or calcined natural pozzolan for use in concrete, Annual Book of ASTM Standards.
45. ASTM, "Standard specification for mixing water used in the production of hydraulic cement concrete," ASTM C1602/C1602M – 22, 2022.

46. TSE, T. (2016). 196–1. Methods of testing cement-Part 1: Determination of strength. Turkish Standards Institute, Ankara.
47. Standardization Administration of China. (2021). Method of testing cements—Determination of strength (GB/T 17671-2021).
48. Chen, S. et al. Elucidating the influence of minimum environmental temperature on freeze-thaw damage behavior of concrete: Wave propagation technology assisted non-destructive structural performance testing. *Constr. Build. Mater.* **487**, 142098. https://doi.org/10.1016/j.conbuildmat.2025.142098 (2025).
49. TS EN 12504–4. (2012). Concrete testing - Part 4: Determination of ultrasonic pulse wave velocity. Turkish Standards Institute (TSE), Ankara.
50. ASTM, C. 592 (2022) ASTM C 597–02. Standard test Method For Pulse Velocity Through Concrete.
51. Lima, H. M., Neto, J. A. D. F., Haach, V. G. & Neto, J. M. Physical and mechanical properties of cement-lime mortar for masonry at elevated temperatures: Destructive and ultrasonic testing. *J. Build. Eng.* **104**, 112291. https://doi.org/10.1016/j.jobe.2025.112291 (2025).
52. Bezerra, A. K. et al. Determination of modulus of elasticity and Poisson's ratio of cementitious materials using S-wave measurements to get consistent results between static, ultrasonic and resonant testing. *Constr. Build. Mater.* **398**, 132456. https://doi.org/10.1016/j.conbuildmat.2023.132456 (2023).
53. Saxena, S., Justnes, H. & Baghban, M. H. Performance evaluation of cement mortars incorporating seawater and calcined marl as sustainable alternatives. *Case Stud. Constr. Mater.* https://doi.org/10.1016/j.cscm.2026.e05841 (2026).
54. Sha, D., Huang, C., Jiao, D., Wang, B. & Pan, B. Mechanical properties and microscopic characterization of coal-based synthetic natural gas slag as supplementary cementitious materials. *J. Build. Eng.* **91**, 109490. https://doi.org/10.1016/j.jobe.2024.109490 (2024).
55. Yannick, T. L. et al. Properties of eco-friendly cement mortar designed with grounded lead glass used as supplementary cementitious material. *Heliyon* https://doi.org/10.1016/j.heliyon.2023.e17536 (2023).
56. Ji, C. et al. Potential of using residual tuff mud to produce low-carbon cement mortar. *Sustain. Mater. Technol.* https://doi.org/10.1016/j.susmat.2025.e01559 (2025).
57. Aodkeng, S. & Chaipanich, A. Compressive strength, characterizations and drying shrinkage mechanism of mortars using calcined clay from different sources. *Case Stud. Constr. Mater.* https://doi.org/10.1016/j.cscm.2025.e04738 (2025).
58. Shen, W. et al. Cleaner production of high-quality manufactured sand and ecological utilization of recycled stone powder in concrete. *J. Cleaner Prod.* **375**, 134146. https://doi.org/10.1016/j.jclepro.2022.134146 (2022).
59. Chaipanich, A., Promwijit, W., Nararueang, A., Aodkeng, S. & Wianglor, K. Utilization of calcareous fly ash with Lopburi calcined clay as high Portland cement replacement supplementary cementitious materials. *Case Stud. Constr. Mater.* https://doi.org/10.1016/j.cscm.2025.e05228 (2025).
60. Wang, J. et al. Innovative utilization of silt clay as a sustainable supplementary cementitious material for energy-efficient cement composites. *J. Build. Eng.* https://doi.org/10.1016/j.jobe.2025.113873 (2025).
61. Adesanya, E. D., Marsh, A. T., Krishnan, S., Yliniemi, J. & Bernal, S. A. Co-calcination of kaolinitic clay and green liquor dregs to produce supplementary cementitious materials. *Case Stud. Constr. Mater.* **22**, e04520. https://doi.org/10.1016/j.cscm.2025.e04520 (2025).
62. Kurt, Z., Ustabaş, İ & Cakmak, T. Novel binder material in geopolymer mortar production: Obsidian stone powder. *Struct. Concr.* **24**(4), 5600–5613. https://doi.org/10.1002/suco.202201089 (2023).
63. Altomare, A., Cuocci, C., Giacovazzo, C., Moliterni, A. & Rizzi, R. 'QUALX : A computer program for qualitative analysis using powder diffraction data'. *J. Appl. Cryst.* **41**(4), 815–817. https://doi.org/10.1107/S0021889808016956 (2008).
64. Altomare, A. et al. QUALX2.0: a qualitative phase analysis software using the freely available database POW_COD. *J. Appl. Cryst.* **48**, 598–603. https://doi.org/10.1107/S1600576715002319 (2015).
65. Burbano-Garcia, C. et al. Short/long term assessment of precast concrete block waste as a supplementary cementitious material: mechanical performance, hydration, and microstructure evolution. *J. Build. Eng.* https://doi.org/10.1016/j.jobe.2025.113868 (2025).
66. Li, X., Lv, X., Zhou, X., Meng, W. & Bao, Y. Upcycling of waste concrete in eco-friendly strain-hardening cementitious composites: Mixture design, structural performance, and life-cycle assessment. *J. Clean. Prod.* **330**, 129911. https://doi.org/10.1016/j.jclepro.2021.129911 (2022).
67. Liu, J., Joseph, S., Rauwoens, P. & Cizer, Ö. Recycling of mixed recycled aggregates as a supplementary cementitious material. *Constr. Build. Mater.* **462**, 139977. https://doi.org/10.1016/j.conbuildmat.2025.139977 (2025).
68. Fernandes, I. V. et al. Valorization of textile sludge for use as supplementary cementitious material–Benefiting processes, pozzolanic activity, and application in no-slump concrete. *Constr. Build. Mater.* **458**, 139619. https://doi.org/10.1016/j.conbuildmat.2024.139619 (2025).
69. Lv, T. et al. Performance of acid-alkali activated dredged sludge as a supplementary cementitious material. *Constr. Build. Mater.* **458**, 139569. https://doi.org/10.1016/j.conbuildmat.2024.139569 (2025).
70. Jin, H. et al. Effects of limestone calcined clay, fly ash and seawater on early hydrating behavior, mechanical properties, microscopic performance and sustainability of eco-friendly cement-based pastes. *J. Therm. Anal. Calorim.* **149**(5), 2087–2107. https://doi.org/10.1007/s10973-023-12823-9 (2024).
71. Abuqasim, S. et al. Examination of porcelain polishing residue as a supplementary cementitious materials. *J. Build. Eng.* https://doi.org/10.1016/j.jobe.2025.112897 (2025).
72. Chen, Z., Luo, K. & Ye, H. Understanding reactivity of calcined marine clay as a supplementary cementitious material through structural transformation of clay minerals. *Cement Concr. Compos.* **160**, 106066. https://doi.org/10.1016/j.cemconcomp.2025.106066 (2025).
73. Li, J. S. et al. Change in re-use value of incinerated sewage sludge ash due to chemical extraction of phosphorus. *Waste Manage.* **74**, 404–412. https://doi.org/10.1016/j.wasman.2018.01.007 (2018).
74. Aramburo, C. H., Pedrajas, C. & Talero, R. Portland cements with high content of calcined clay: Mechanical strength behaviour and sulfate durability. *Materials* **13**(18), 4206. https://doi.org/10.3390/ma13184206 (2020).
75. Dhar, M. & Bishnoi, S. Influence of calcination temperature on the physical and chemical characteristics of kaolinitic clays for use as supplementary cementitious materials. *Cem. Concr. Res.* **178**, 107464. https://doi.org/10.1016/j.cemconres.2024.107464 (2024).
76. Avci, E. et al. Quarry waste clays as supplementary cementitious materials: Mineralogical evolution and pozzolanic performance after thermal activation. *Appl. Clay Sci.* **281**, 108085. https://doi.org/10.1016/j.clay.2025.108085 (2026).
77. de Oliveira, A. M., Oliveira, A. P., Vieira, J. D., Junior, A. N. & Cascudo, O. Study of the development of hydration of ternary cement pastes using X-ray computed microtomography, XRD-Rietveld method, TG/DTG, DSC, calorimetry and FTIR techniques. *J. Build. Eng.* **64**, 105616. https://doi.org/10.1016/j.jobe.2022.105616 (2023).
78. Yang, X. et al. Effects of GBFS content and curing methods on the working performance and microstructure of ternary geopolymers based on high-content steel slag. *Constr. Build. Mater.* **410**, 134128. https://doi.org/10.1016/j.conbuildmat.2023.134128 (2024).
79. Zajac, M., Bremeier, R., Deja, J., Król, M. & Haha, M. B. Carbonation hardening of Portland cement with recycled supplementary cementitious materials. *Cement Concr. Compos.* **157**, 105904. https://doi.org/10.1016/j.cemconcomp.2024.105904 (2025).
80. Zhou, D., Wang, R., Tyrer, M., Wong, H. & Cheeseman, C. Sustainable infrastructure development through use of calcined excavated waste clay as a supplementary cementitious material. *J. Clean. Prod.* **168**, 1180–1192. https://doi.org/10.1016/j.jclepro.2017.09.098 (2017).

81. Li, Z., Ma, G., Zheng, D. & Zhang, X. Effect of Fe2O3 on the crystallization behavior, microstructure and properties of glass-ceramics prepared from the modified tailings after reduction of copper slag. *Mater. Today Commun.* **31**, 103516. https://doi.org/10.1016/j.mtcomm.2022.103516 (2022).
82. Liu, J. et al. Calcined oil shale residue as a supplementary cementitious material for ordinary Portland cement. *Constr. Build. Mater.* **306**, 124849. https://doi.org/10.1016/j.conbuildmat.2021.124849 (2021).
83. de Godoy, L. G. G., Rohden, A. B., Garcez, M. R., Da Dalt, S. & Gomes, L. B. Production of supplementary cementitious material as a sustainable management strategy for water treatment sludge waste. *Case Stud. Constr. Mater.* **12**, e00329. https://doi.org/10.1016/j.cscm.2020.e00329 (2020).
84. Mottakin, M. et al. Evaluation of textile effluent treatment plant sludge as supplementary cementitious material in concrete using experimental and machine learning approaches. *J. Build. Eng.* **96**, 110627. https://doi.org/10.1016/j.jobe.2024.110627 (2024).
85. Chen, T. T., Wang, W. C. & Wang, H. Y. Mechanical properties and ultrasonic velocity of lightweight aggregate concrete containing mineral powder materials. *Constr. Build. Mater.* **258**, 119550. https://doi.org/10.1016/j.conbuildmat.2020.119550 (2020).
86. Chao-Lung, H., Le Anh-Tuan, B. & Chun-Tsun, C. Effect of rice husk ash on the strength and durability characteristics of concrete. *Constr. Build. Mater.* **25**(9), 3768–3772. https://doi.org/10.1016/j.conbuildmat.2011.04.009 (2011).
87. Bheel, N. et al. Synergistic effect of recycling waste coconut shell ash, metakaolin, and calcined clay as supplementary cementitious material on hardened properties and embodied carbon of high strength concrete. *Case Stud. Constr. Mater.* **20**, e02980. https://doi.org/10.1016/j.cscm.2024.e02980 (2024).
88. Khan, M. S. et al. Enhancing rigid pavement performance: Experimental study and design optimization of bentonite clay-blended concrete with a focus on durability. *Case Stud. Constr. Mater.* **22**, e04641. https://doi.org/10.1016/j.cscm.2025.e04641 (2025).
89. Ulucan, M. & Cebeci, I. Performance and sustainability of self-compacting mortars made with recycled aggregate and supplementary cementitious materials. *Sustain. Chem. Pharm.* **46**, 102080. https://doi.org/10.1016/j.scp.2025.102080 (2025).
90. Ghanim, A. A., Rahman, F. U., Adil, W., Zeyad, A. M. & Magbool, H. M. Experimental investigation of industrial wastes in concrete: Mechanical and microstructural evaluation of pumice powder and fly ash in concrete. *Case Stud. Constr. Mater.* **18**, e01999. https://doi.org/10.1016/j.cscm.2023.e01999 (2023).
91. Adil, W., Rahman, F. U., Abdullah, G. M., Tayeh, B. A. & Zeyad, A. M. Effective utilization of textile industry waste-derived and heat-treated pumice powder in cement mortar. *Constr. Build. Mater.* **351**, 128966. https://doi.org/10.1016/j.conbuildmat.2022.128966 (2022).
92. Liu, S. et al. Sustainable use of waste oyster shell powders in a ternary supplementary cementitious material system for green concrete. *Materials* **15**(14), 4886. https://doi.org/10.3390/ma15144886 (2022).
93. Hu, Q. et al. Direct three-dimensional observation of the microstructure and chemistry of C3S hydration. *Cement concrete Res.* **88**, 157–169. https://doi.org/10.1016/j.cemconres.2016.07.006 (2016).
94. Zahid, F. B., Ong, Z. C. & Khoo, S. Y. A review of operational modal analysis techniques for in-service modal identification. *J. Braz. Soc. Mech. Sci. Eng.* **42**(8), 398. https://doi.org/10.1007/s40430-020-02470-8 (2020).
95. Stochino, F. et al. Structural identification from operational modal analysis: the case of steel structures. *Buildings* **13**(2), 548. https://doi.org/10.3390/buildings13020548 (2023).
96. Taskaya, S. & Taskaya, S. Investigation of static structure effect according to axial coordinates by using finite element method in Ansys workbench software of AISI 310 austenitic stainless cylindrical model steel. *Int. J. Sci. Eng. Sci.* **2**(11), 65–70 (2018).
97. Zhao, Z. & Kang, Z. Automate topology optimization based on force density method for form-finding of branching structures. *J. Building Eng.* https://doi.org/10.1016/j.jobe.2025.113254 (2025).
98. PEER 2014. Pacific Earthquake Engineering Research Center, Ground Motion Database, University of California, Berkeley, USA. http://ngawest2.berkeley.edu/.
99. Kurt, Z., Ateş, Ş. (2019). Earthquake analysis of hospıtal building with seismic isolation to Turkey Building Earthquake Code 2018. In: *Internatıonal Civil Engineering and Architecture Conference 2019.*
100. ANSYS 16.0. Swanson Analysis Systems Inc., Houston, PA, USA (2016).

Acknowledgements
Funding This study has been supported by the Recep Tayyip Erdoğan University Development Foundation (Grant number: 02026002013120)

Author contributions
Z.K.: Investigation, methodology, conceptualization, visualization, writing—original draft preparation, writing—review and editing.

Declarations

Competing interests
The authors declare no competing interests.

Additional information
Correspondence and requests for materials should be addressed to Z.K.

Reprints and permissions information is available at www.nature.com/reprints.

Publisher's note Springer Nature remains neutral with regard to jurisdictional claims in published maps and institutional affiliations.

Open Access This article is licensed under a Creative Commons Attribution-NonCommercial-NoDerivatives 4.0 International License, which permits any non-commercial use, sharing, distribution and reproduction in any medium or format, as long as you give appropriate credit to the original author(s) and the source, provide a link to the Creative Commons licence, and indicate if you modified the licensed material. You do not have permission under this licence to share adapted material derived from this article or parts of it. The images or other third party material in this article are included in the article's Creative Commons licence, unless indicated otherwise in a credit line to the material. If material is not included in the article's Creative Commons licence and your intended use is not permitted by statutory regulation or exceeds the permitted use, you will need to obtain permission directly from the copyright holder. To view a copy of this licence, visit http://creativecommons.org/licenses/by-nc-nd/4.0/.

© The Author(s) 2026